In Proc. 11th International Conference on Flow-Induced Vibrations and Noise, Gonzalez, Belfroid, and Golliard (eds), The Hague, The Netherlands, 2016, pp. 239-246. (conf. July 4-6, 2016). ISBN-978-90-9029803-0

REYNOLDS NUMBER EFFECTS ON FLOW AROUND A CYLINDER IN FIGURE-EIGHT-PATH MOTION

László Baranyi
Department of Fluid and Heat Engineering,
University of Miskolc,
3515 Miskolc-Egyetemváros, Hungary
E-mail: arambl@uni-miskolc.hu

ABSTRACT

Forced figure-eight motion of a cylinder placed in an otherwise uniform stream was investigated for both clockwise (CW) and anticlockwise (ACW) directions of orbit in this two-dimensional numerical study for Reynolds numbers Re=50 to 180. Mechanical energy transfer E between the cylinder and fluid, and time-mean and rms values of force coefficients were investigated in the lock-in domain against frequency ratio up to FR=f_v/St$_0$=1 using a thoroughly tested finite difference code. It was found that both the direction of orbit and Re have a major effect on lift and mechanical energy transfer. The time-mean value of lift was practically zero over the investigated domain for the ACW case, and mainly positive for the CW orbit and increased with Re. E values were mainly positive for the ACW case, meaning a potential risk of vortex-induced vibration (VIV). E values were negative for the CW case for all Re (no VIV danger).

NOMENCLATURE

$a_{0x,y}$	cylinder acceleration in x or y directions, respectively, non-dimensionalized by U^2/d
$A_{x,y}$	amplitude of oscillation in x or y directions, respectively, non-dimensionalized by d
C_D	drag coefficient, $2F_D/(\rho U^2 d)$, dimensionless
C_L	lift coefficient, $2F_L/(\rho U^2 d)$, dimensionless
d	cylinder diameter (m), length scale
D	dilation, non-dimensionalized by U/d
E	mechanical energy transfer, dimensionless
$\mathbf{F}$	$=F_D\,\mathbf{i} + F_L\,\mathbf{j}$, force per unit length of cylinder (N/m)
F_D	drag per unit length of cylinder (N/m)
F_L	lift per unit length of cylinder (N/m)
FR	frequency ratio, f_v/St$_0$, dimensionless
$f_{x,y}$	oscillation frequency in x or y directions, respectively, non-dimensionalized by U/d
f_v	vortex shedding frequency (1/s)
$\mathbf{i}$, $\mathbf{j}$	unit vectors in x and y directions, dimensionless
p	pressure, non-dimensionalized by ρU^2
Re	Reynolds number, $U\,d/\upsilon$, dimensionless
R	radius, non-dimensionalized by d
St	non-dimensional vortex shedding frequency, $f_v\,d/U$
t	time, non-dimensionalized by d/U
T	motion period, $T=1/f_y$, dimensionless
U	free stream velocity, velocity scale (m/s)
u, v	velocities in x or y directions, respectively, non-dimensionalized by U
$\mathbf{v_0}$	$=v_{0x}\,\mathbf{i} + v_{0y}\,\mathbf{j}$, cylinder velocity, non-dimensionalized by U
x,y	Cartesian co-ordinates, non-dimensionalized by d
υ	kinematic viscosity (m^2/s)
ρ	fluid density (kg/m^3)

Subscripts

fb	fixed body
D	drag
L	lift
rms	root-mean-square value
x, *y*	components in x and y directions
v	vortex
0	for cylinder motion; for stationary cylinder at same Re

INTRODUCTION

Flow around cylinders oscillating in transverse or in-line directions to the main stream has long been in the focus of attention. In real life, however, this pure one-degree-of-freedom motion is relatively uncommon; often both transverse and in-line motions occur simultaneously, resulting in a two-degree-of-freedom (2-DoF) motion.

Studies dealing with 2-DoF forced cylinder motion basically fall into two groups: the first is when the frequencies are identical in x and y direction (f_x=f_y), leading to an elliptical path, as e.g. in [1-2]. The second is when the frequency of in-line oscillation is double that of the transverse oscillation (f_x=2f_y), resulting in a figure-8 path. Two examples of experimental studies in this field are [3] for free vibration and [4] for forced vibration. Numerical studies often place a cylinder in forced motion in order to gain an approximation of fluid-structure interaction. While this is a simplified model, and a direct relationship between free and forced vibration is difficult to confirm [5], it is a suitable starting point for investigation of this complex phenomenon. In their numerical study [6] identified the lock-in thresholds of a cylinder in forced transverse oscillation and found that oscillation amplitude values for an elastically-supported

cylinder fell within these thresholds, indicating that prediction is possible by forced cylinder motion.

In [7] the authors investigated flow around a mechanically oscillated cylinder following a figure-eight path at Reynolds number Re=400 while varying the transverse amplitude of oscillation. They found that the orientation of the motion (clockwise (CW) or anticlockwise (ACW) orbit, as seen in the upper loop of the figure-eight) influences the results, generally leading to higher force coefficients and power transfer for the ACW orientation, meaning an increased chance of vortex-induced vibration (VIV) for a cylinder in free vibration. In their numerical study [8] the authors investigated the sensitivity of two-dimensional flow past a transversely oscillating cylinder to streamwise cylinder oscillation at Re=150. The frequency of cylinder oscillation in the streamwise direction was double that of the transverse direction, resulting in a figure-eight cylinder path. They carried out investigations for both CW and ACW directions of orbit (in the upper loop of figure-eight) at frequency ratios FR=f_y/St$_0$=0.9 and 1 at amplitude ratios A_x/A_y=0 to 0.5 while the dimensionless transverse amplitude was varied from 0.1 to 0.6. They found that while the energy transfer is negative for the CW orbit, it is positive for most of the parameter domain for ACW orbit.

A numerical study of the present author [9] dealt with forced figure-eight motion for Re=200, 250 and 300 against frequency ratio, for a slender figure-eight path with amplitude ratio A_x/A_y=0.28 for both CW and ACW orientations. For the CW orbit a single sudden change in the time-mean of lift indicating a switch in the vortex structure was identified for both Re=250 and 300. The mechanical energy transfer E between fluid and cylinder was found to be negative for all investigated CW orbit cases, meaning that there is no danger of VIV in this case. However, when the cylinder was orbiting in the ACW direction the results were different: zero time-mean of lift and positive E for all cases.

In addition to studies looking at the effect of frequency ratio, work has been carried out on the effect of amplitude ratio for figure-eight cylinder motion at Re=150 [8, 10]. However, to the best knowledge of the author no detailed investigation into the effect of Re has been carried out.

The objective of this study is to fill this gap by investigating the flow around a cylinder following a figure-eight path for both directions of orbit for Re=50 to 180 against frequency ratio. Time-mean and rms values of force coefficients and mechanical energy transfer values for a cylinder following a symmetrical figure-8 path are compared by direction of orbit in order to determine the influence of direction on flow behavior in the given Reynolds number domain.

GOVERNING EQUATIONS, COMPUTATIONAL SETUP

A non-inertial system fixed to the cylinder is used to compute the two-dimensional (2D) flow around a circular cylinder placed in a uniform stream and forced to oscillate in transverse or in-line direction, or both. The non-dimensional Navier-Stokes equations for incompressible Newtonian fluid, the equation of continuity and the Poisson equation for pressure can be written as follows:

$$\frac{\partial u}{\partial t}+u\frac{\partial u}{\partial x}+v\frac{\partial u}{\partial y}=-\frac{\partial p}{\partial x}+\frac{1}{\mathrm{Re}}\nabla^2 u-a_{0x}, \qquad (1)$$

$$\frac{\partial v}{\partial t}+u\frac{\partial v}{\partial x}+v\frac{\partial v}{\partial y}=-\frac{\partial p}{\partial y}+\frac{1}{\mathrm{Re}}\nabla^2 v-a_{0y}, \qquad (2)$$

$$D=\frac{\partial u}{\partial x}+\frac{\partial v}{\partial y}=0, \qquad (3)$$

$$\frac{\partial^2 p}{\partial x^2}+\frac{\partial^2 p}{\partial y^2}=2\left[\frac{\partial u}{\partial x}\frac{\partial v}{\partial y}-\frac{\partial u}{\partial y}\frac{\partial v}{\partial x}\right]-\frac{\partial D}{\partial t}. \qquad (4)$$

In these dimensionless equations, u and v are the x and y components of velocity, t is time, p is the pressure, Re is the Reynolds number and D is the dilation. Although D is theoretically equal to 0 for incompressible fluids from Eqn. (3), it is kept in Eqn. (4) to avoid the accumulation of numerical errors. In Eqns. (1) and (2) a_{0x} and a_{0y} are the x and y components of cylinder acceleration, respectively.

On the cylinder surface, no-slip boundary condition is used for the velocity and a Neumann type boundary condition for the pressure. Potential flow is assumed at the far region. The author is aware that this assumption is not valid for the narrow wake at the outlet boundary; earlier numerical analysis and tests [1] showed, however, that this assumption results in only a small distortion of the velocity field near the outlet boundary of the wake region.

Boundary-fitted coordinates are used to impose the boundary conditions accurately. The physical domain bounded by two concentric circles is mapped onto a rectangular computational domain with equidistant spacing in both directions. In the physical domain logarithmically spaced radial cells are used, ensuring a fine grid scale near the cylinder wall and a coarse grid in the far field. The transformed governing equations and boundary conditions are solved by finite difference method. Space derivatives are approximated by fourth order central differences, except for the convective terms for which a third order modified upwind scheme is used. The Poisson equation for pressure is solved by the successive over-relaxation (SOR) method. The Navier-Stokes equations are integrated explicitly and continuity is satisfied at every time step (see [1]).

The 2D code developed by the author has been extensively tested against experimental and computational results for a stationary cylinder ([11]) and computational results for cylinders oscillating in transverse and in-line directions or following a circular path, including those of [12-14], with good agreement being found (see [1]). In this study the dimensionless time step is 0.0005, the number of grid points is 361x292 (peripheral x radial), and the physical domain is characterized by R_2/R_1=160.

This numerical study investigates the behavior of flow past a cylinder placed in a uniform stream with its axis perpendicular to the velocity vector of the main flow. The

cylinder is oscillated mechanically in both in-line and transverse directions in relation to the uniform stream. The layout of the cylinder path can be seen in Fig. 1. Here U is the free stream velocity, d is the cylinder diameter, and A_x and A_y are the dimensionless amplitudes in x and y directions, respectively. Quantities are non-dimensionalized by the combination of U and d. The displacements of the forced cylinder motion x_0, y_0 in x and y directions are given by

$$x_0 = A_x \sin(2\pi f_x t + \Theta), \tag{5}$$

$$y_0 = A_y \sin(2\pi f_y t), \tag{6}$$

where A_x, A_y and f_x, f_y are the dimensionless amplitudes and frequencies of the cylinder oscillation in x and y directions, respectively. If $f_x = 2f_y$, Eqns. (5) and (6) ensure a figure-eight or distorted figure-eight path. Depending on the phase angle Θ between cylinder motions in x and y directions, clockwise (CW) or anticlockwise (ACW) orbit can be obtained in the upper loop of the figure-eight:

$$f_x = 2f_y; \quad \Theta = \pi, \quad \text{(for CW)}, \tag{7}$$

$$f_x = 2f_y; \quad \Theta = 0, \quad \text{(for ACW)}. \tag{8}$$

Figure 1 also shows the velocity vectors along the cylinder paths near y_0=0 for both CW (red filled arrows) and ACW (empty black arrows) orbits. Note that although the two paths are symmetric about x_0 axis, the configuration is not symmetric about the y_0 axis. As shown in the figure, the x component of the cylinder velocity $v_{0x} = \mathrm{d}x_0/\mathrm{d}t < 0$ for CW and $v_{0x} = \mathrm{d}x_0/\mathrm{d}t > 0$ for ACW orbits near y_0=0. At both the top and bottom of the trajectory the cylinder moves in the direction of the main flow velocity U for CW orbit, and against the main flow for ACW orbit. Hence, the two directions of orbits lead to substantially different force coefficients and energy transfer between fluid and cylinder, as is shown later.

The frequency ratio

$$\mathrm{FR} = f_y / \mathrm{St}_0, \tag{9}$$

where St_0 is the dimensionless vortex shedding frequency or Strouhal number belonging to a stationary cylinder at the given Reynolds number. In this study the Strouhal numbers belonging to different Re values are taken from [15].

Throughout this paper the lift (C_L) and drag (C_D) coefficients used do not contain the inertial forces originating from the non-inertial system fixed to the moving cylinder. These coefficients are often termed 'fixed body' coefficients (see [12]). The two sets of coefficients can be written as

$$C_L = C_{Lfb} + \frac{\pi}{2} a_{0y}, \; C_D = C_{Dfb} + \frac{\pi}{2} a_{0x}, \tag{10}$$

where subscript *fb* stands for fixed body (understood in an inertial system) [15]. In Eqn. (10) (and also in Eqns. (1) and (2)) a_{0x} and a_{0y} accelerations are the second time derivatives of cylinder displacements x_0, y_0 given in Eqns. (5) and (6). Since a_{0x} and a_{0y} are T-periodic functions, their time-mean (TM) values vanishes, resulting in identical TM values for lift and drag in the two systems. Naturally, the rms values of force coefficients will be somewhat different in the inertial and non-inertial systems.

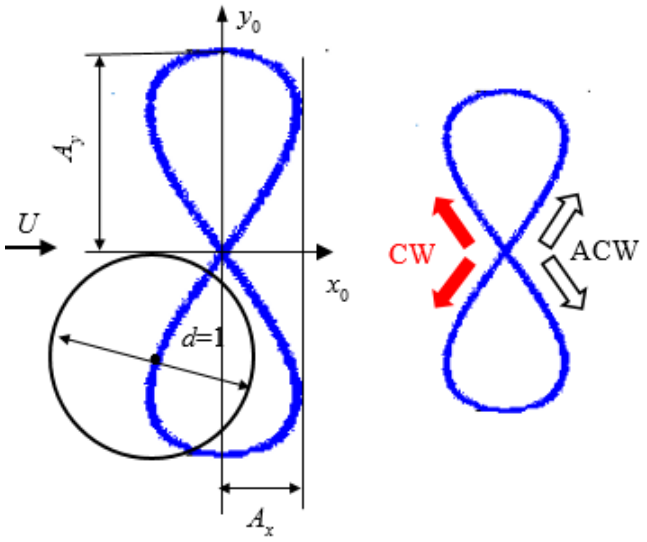

FIGURE 1: LAYOUT FOR FIGURE-EIGHT PATH

The mechanical energy transfer E originally introduced in [17] for a transversely oscillating cylinder is extended for general 2-DoF cylinder motion in [1]:

$$E = \frac{2}{\rho U^2 d^2} \int_0^T \mathbf{F} \cdot \mathbf{v}_0 \, \mathrm{d}t = \int_0^T \left(C_D \, v_{0x} + C_L \, v_{0y} \right) \mathrm{d}t. \tag{11}$$

Since the frequencies in the two directions are different (see Eqns. (7) and (8)) the larger period $T = T_y = 1/f_y$ is chosen here. In Eqn. (11) $\mathbf{F}$ is the force vector per unit length of cylinder, $\mathbf{v_0} = (v_{0x}, v_{0y})$ the velocity vector of the cylinder.

In this study several Reynolds numbers are investigated between Re=50 and 180, and the frequency ratios FR is varied between the lower lock-in threshold value and 1. During the investigation oscillation frequencies are set at $f_x = 2f_y$, and oscillation amplitudes are kept constant at A_x=0.14 and A_y=0.5 to ensure a slender figure-eight path. All computations are carried out for both directions of orbit.

COMPUTATIONAL RESULTS AND DISCUSSION

In this study computations are carried out for a cylinder in forced motion following a fixed slender figure-eight path for both clockwise (CW) and anticlockwise (ACW) orbits in the upper loop of figure-eight path at low Reynolds numbers. Time-mean (TM) and root-mean-square (rms) values of lift and drag coefficients and mechanical energy transfer E are shown against frequency ratio FR in the lock-in domain, basically from FR=0.65 to FR=1 (i.e., when $f_y = \mathrm{St}_0$). One pair

of vorticity contours belonging to identical Re, FR, A_x, A_y values and cylinder position for the CW and ACW orbits is also shown, demonstrating the substantial difference in the vortex structures.

Time-mean and rms Values of Force Coefficients

Earlier results of the present author [9] motivating the current study are shown in Fig. 2. The clockwise (CW) curves (empty signals in the figure) have one jump each for Re=250 and 300, showing a sudden switch in vortex structure. These curves are similar to those for in-line cylinder motion, and the vortex switch is probably due to a symmetry-breaking bifurcation [18]. The vortex shedding mode [19] is P+S (one pair of vortices and a single vortex are shed in one period). Figure 2 also shows the TM of lift for the ACW case (filled signals in the figure) for the three Reynolds numbers found to be zero in the investigated domain due to the regular 2S vortex shedding (two single vortices are shed in a period).

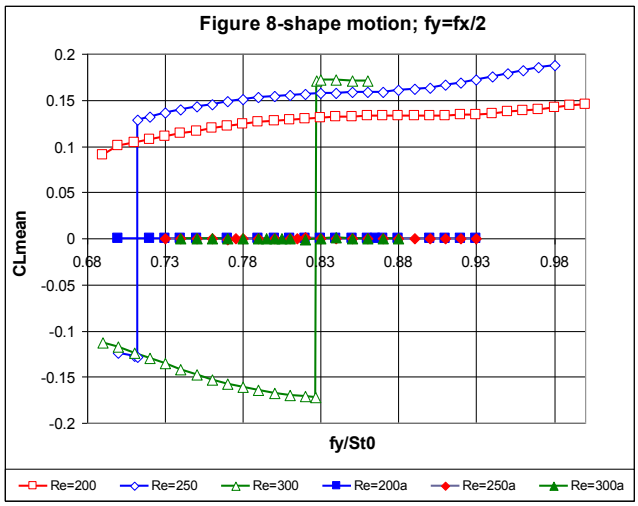

FIGURE 2: TIME-MEAN OF LIFT COEFFICIENT VS. FREQUENCY RATIO FOR CW (RE=200, 250, 300) AND ACW (RE=200a, 250a, 300a) ORBITS ([9])

Figure 3 shows results of the current study for the TM of lift against frequency ratio for different Reynolds numbers (Re=50–180) for CW orientation of orbit. It can be seen that unlike larger Re values (cf. Fig. 2) only non-negative TM values were obtained in the parameter domain investigated. The TM of lift is fully positive only for Re=180 shown in Fig. 3. As Re decreases the TM of lift decreases and below some FR value the TM of lift becomes zero (see e.g. curves for Re=110, 114, 120 and 140 in Fig. 3). For around Re=100 and below the TM of lift is zero over the whole investigated FR domain, similarly to the ACW orbits shown in Fig. 2.

Figure 4 shows that the TM of lift for the ACW orbit is practically zero below FR=0.97, similarly to the Re=200, 250 and 300 cases shown in Fig. 2 (filled signals). In Fig. 4, however, a sudden jump in the TM of lift curve can be seen at Re=0.97 for Re=180 and a small change at FR=0.98 for Re=160. By comparing Figs. 3 and 4 it can be concluded that the TM of lift for the CW and ACW orbits are very different.

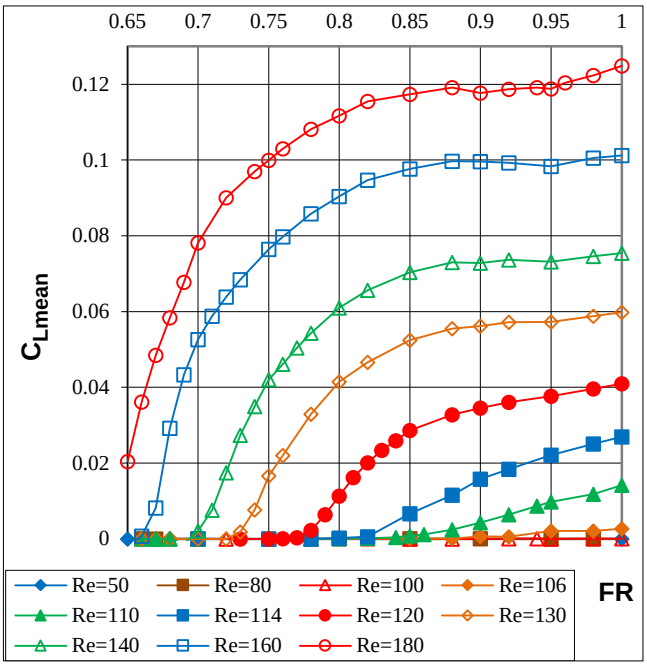

FIGURE 3: TIME-MEAN OF LIFT VS. FREQUENCY RATIO FOR CW ORBITS AT DIFFERENT RE

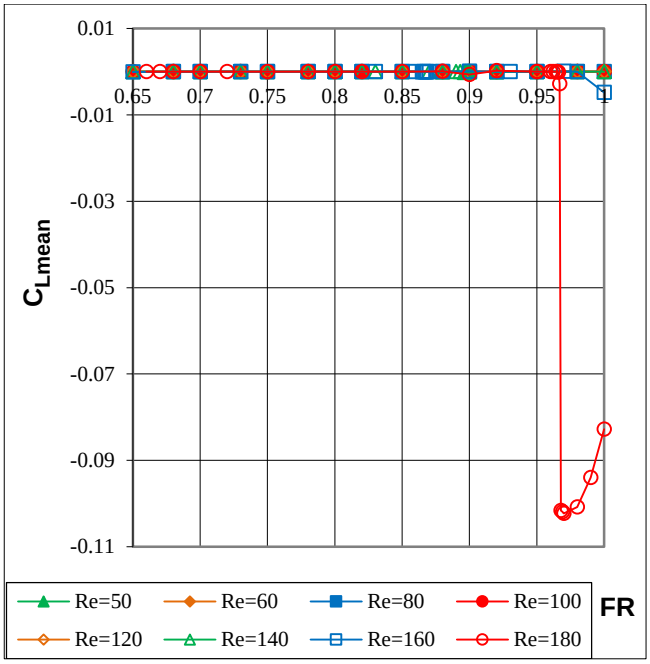

FIGURE 4: TIME-MEAN OF LIFT VS. FREQUENCY RATIO FOR ACW ORBIT AT DIFFERENT RE

To illustrate the difference, computed vorticity contours are shown in Figure 5 for Re=180 at FR=0.85 for CW (top) and for ACW (bottom) orbits, in both cases belonging to the topmost cylinder position (cf. Figs. 3 and 4). Gray indicates negative vorticity values (rotating clockwise) and black is

positive (anticlockwise). The vorticity contours are taken at the dimensionless times of t=100T=615.0840 for the CW case and at t=100.5T=618.1591 (shifted by half a period) for ACW. In the top figure (CW orbit) the vortex shedding mode is P+S; one positive and one negative vortex is shed at the upper part and a single positive vortex at the lower part of the cylinder during a vortex shedding period. For this case the time-mean of lift is positive (=0.1174) (see Fig. 3). The vortex shedding mode for ACW (bottom) looks like 2S; one positive and one negative vortex is shed. In this case the TM of lift is zero (see Fig. 4).

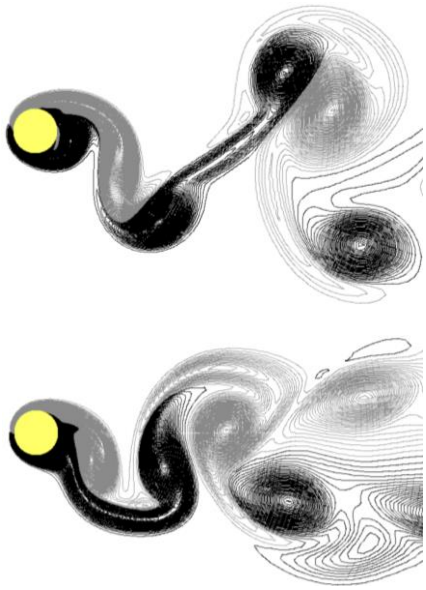

FIGURE 5: VORTICITY CONTOURS FOR CW (TOP) AND ACW (BOTTOM) ORBITS AT TOPMOST CYLINDER POSITION (RE=180; FR=0.85)

For the ACW orbit the in-line component of the cylinder velocity is positive over the larger part of the orbit (see Fig. 1); it is still unclear whether this leads to the 2S vortex shedding mode (which results in zero TM of lift over the largest part of the Re domain [19]). In contrast, in the CW orbit the in-line component of the cylinder velocity is negative (against the main flow) over the larger part of its orbit, which may result in P+S vortex shedding mode for the larger Re values investigated. Under Re=100 the TM of lift is also zero (see Fig. 3) and 2S shedding is found for the CW orbit, just as in the case of the ACW orbit.

Figure 6 shows the TM of drag against FR for the CW orbit for several Reynolds numbers from 50 to 180. The TM of drag increases with both FR and Re except in the lower Re and FR domains, where the opposite is true (the largest TM of drag is for Re=50). The curves belonging to different Re numbers are smooth and monotonous functions of FR.

Although the general trend is similar, this is not quite true for the TM of drag plotted against FR for the ACW case at different Reynolds numbers and shown in Fig. 7. Some small jumps can be seen in the curve for Re=180 at FR=0.97 (like in Fig. 4) and for Re=140 and 160. The curves spread more for larger FR values than for the CW case, and the TM of drag values is also somewhat higher.

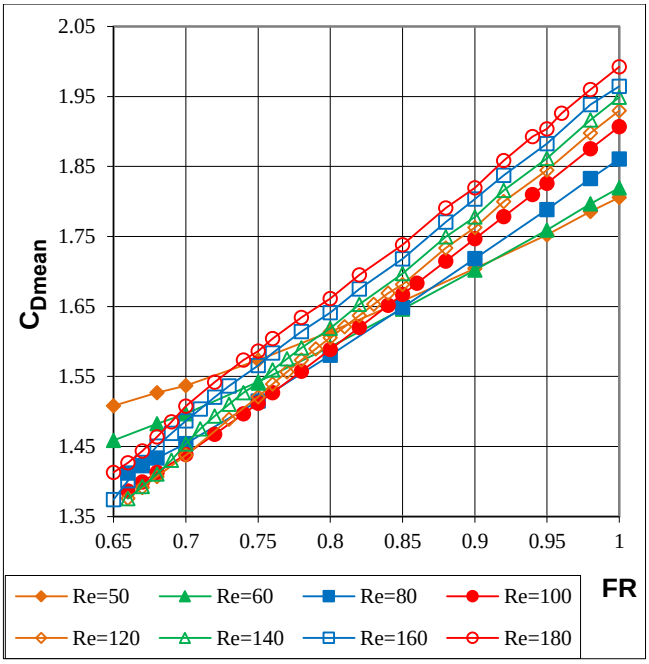

FIGURE 6: TIME-MEAN OF DRAG VS. FREQUENCY RATIO FOR CW ORBIT AT DIFFERENT RE

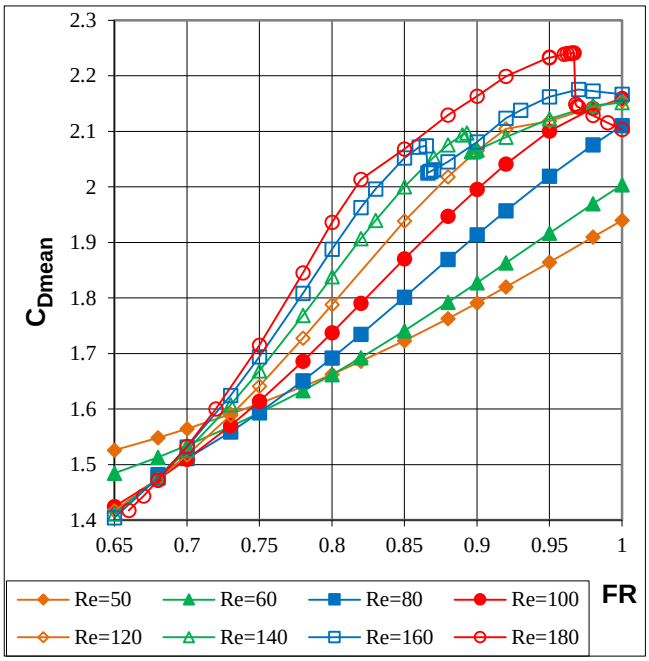

FIGURE 7: TIME-MEAN OF DRAG VS. FREQUENCY RATIO FOR ACW ORBIT AT DIFFERENT RE

The rms values of lift and drag are also investigated. Figure 8 shows the rms of fixed body (free of inertial forces) lift against FR for the CW orbit for Re from 50 to 180. The rms of lift tends to increase with both FR and Re. The threshold value for lock in for the Re=80–140 curves is FR=0.66; all other curves belong to locked-in states over the FR=0.65 to 1 domain. The maximum value of rms of lift is 0.76 (at Re=180; FR=1) over the parameter domain.

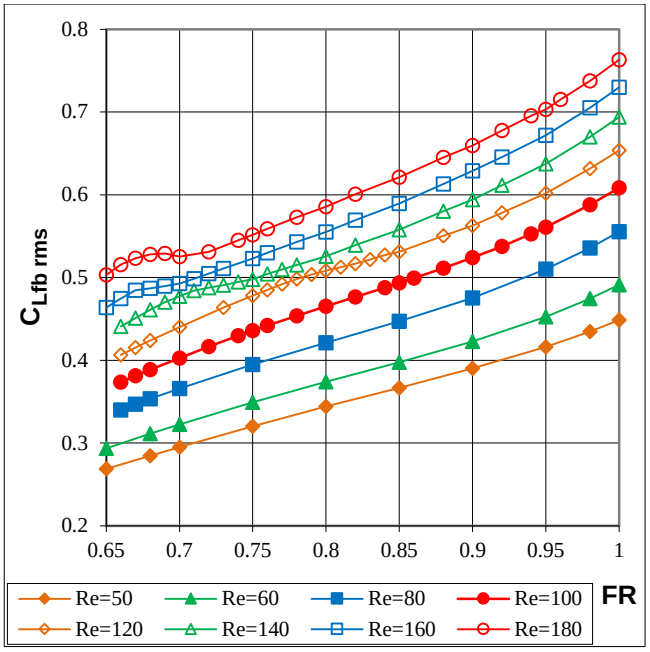

FIGURE 8: RMS OF LIFT VS. FREQUENCY RATIO FOR CW ORBIT AT DIFFERENT RE

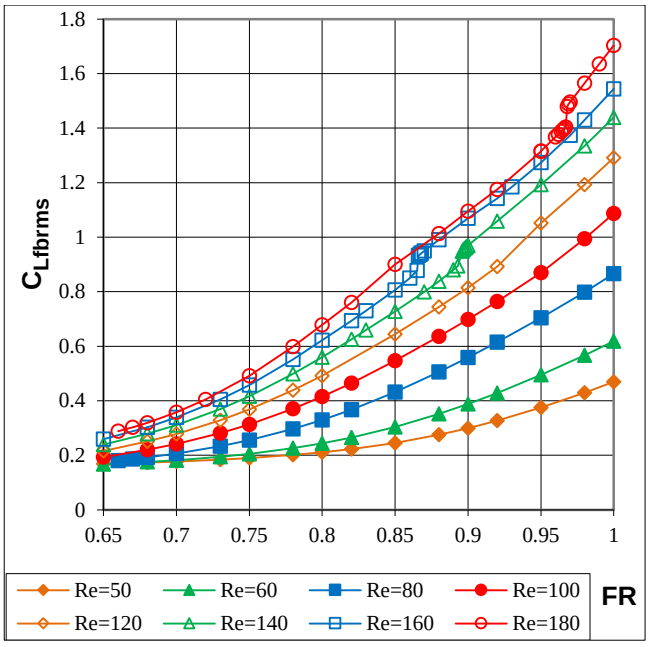

FIGURE 9: RMS OF LIFT VS. FREQUENCY RATIO FOR ACW ORBIT AT DIFFERENT RE

Figure 9 shows the rms of fixed body lift coefficient against frequency ratio FR for the ACW orbit. Again, the rms of lift increases with both Re and FR, but there are some differences compared to the results for the CW orbit: (a) the distance between the curves at fixed Re values increases with FR; (b) there are irregularities in the curves for higher Reynolds numbers; (c) the maximum value of rms of lift is 1.70 (compared to 0.76 for the CW orbit).

Rms values of drag for CW orbit are shown in Fig. 10. Curves belonging to different Reynolds numbers are strictly monotonous functions of FR. The rms of drag increases with Re and FR to a maximum of 2.34. The rms of fixed body drag against frequency ratio FR for the ACW orbit (not shown here) shows similar trends to the CW case. A small difference is that the maximum value of rms drag is 1.71.

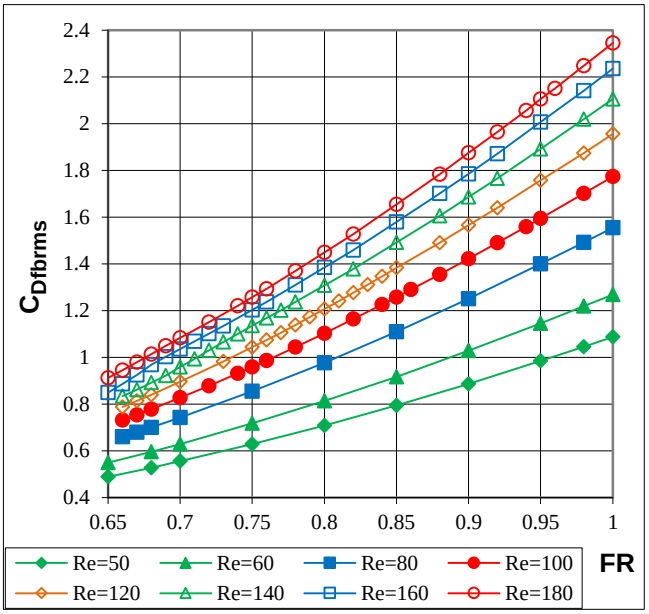

FIGURE 10: RMS OF DRAG VS. FREQUENCY RATIO FOR CW ORBIT AT DIFFERENT RE

Mechanical Energy Transfer

Earlier, the mechanical energy transfer *E* between fluid and cylinder was found to be negative for the clockwise (CW) cylinder orbit at Re=200, 250 and 300 in the investigated frequency ratio FR domain [9] (see empty signals in Fig. 11). This means that there is no danger of vortex-induced vibration (VIV) in the corresponding free vibration case. However, when the cylinder was orbiting in the ACW direction the results were very different; only positive *E* values were found for all investigated cases (see filled signals in Fig. 11) which means risk of VIV.

E is shown in Fig. 12 for both CW and ACW orbits against FR for Reynolds numbers between 50 and 180. It can be seen in the figure that all values are negative for the CW orbit (lower set of curves) over the investigated parameter domain. It can also be observed that the approximate trend is that *E* decreases with both FR and Re. This is not true, however, for the small domain of Re=140, 60 and 180 when FR < 0.73. *E* being negative means that there is no potential danger of VIV of an equivalent elastically supported cylinder for CW orbits at the given amplitude ratio over the investigated Re and FR domain [6]. As can be seen in Fig. 12, *E* curves for the ACW orbit (upper set of curves in the figure) are substantially different from those belonging to CW orbit. As a general trend it can be stated that *E* decreases monotonously with Re, yielding negative *E* values for small

Re values. For example the whole curve remains below zero for Re=50. The danger of VIV decreases with decreasing Re for the ACW orbit. Still, over the larger part of the domain E is positive, meaning there is risk of VIV.

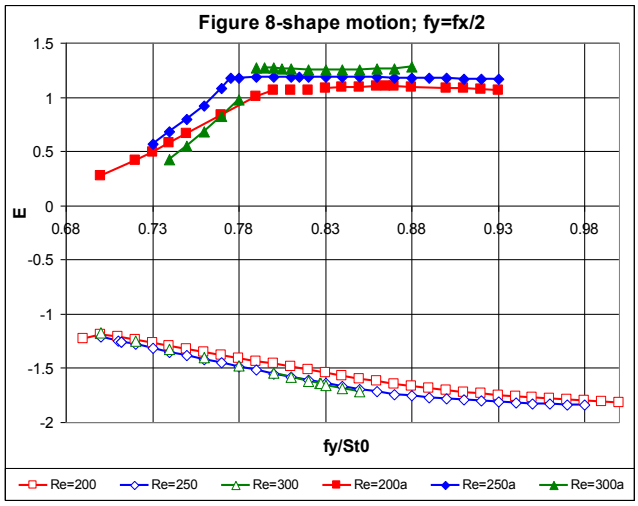

FIGURE 11: MECHANICAL ENERGY TRANSFER VS. FREQUENCY RATIO FOR CW (RE=200, 250, 300) AND ACW (RE=200a, 250a, 300a) ORBITS ([9])

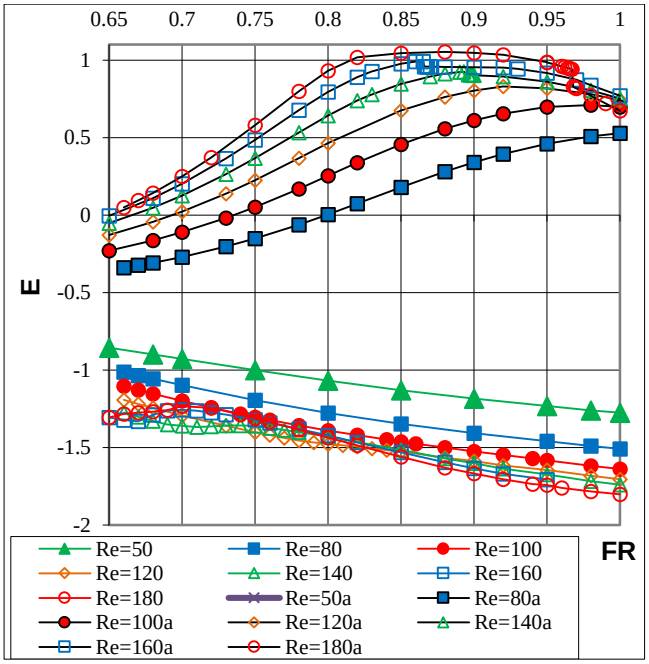

FIGURE 12: MECHANICAL ENERGY TRANSFER VS. FREQUENCY RATIO FOR CW AND ACW ORBITS AT DIFFERENT RE

To see the effect of Re and FR on the mechanical energy transfer more clearly for the ACW orbit, Fig. 13 zooms in on ACW results (cf. top set of curves in Fig. 12). Some sudden changes or jumps can be seen at the top right side of the figure for Re=140, 160 and 180. This probably indicates a switch in the vortex structure [9, 10, 17].

Another difference between results for CW and ACW orbits is in their behavior as FR tends to unity. For CW orbit no significant difference in the dynamics could be detected. The same can be said for the ACW orbits below Re=140 (considering the parameter domain investigated). On the other hand, for ACW orbits above Re=140 jumps can be seen in E, TM and rms of force coefficients.

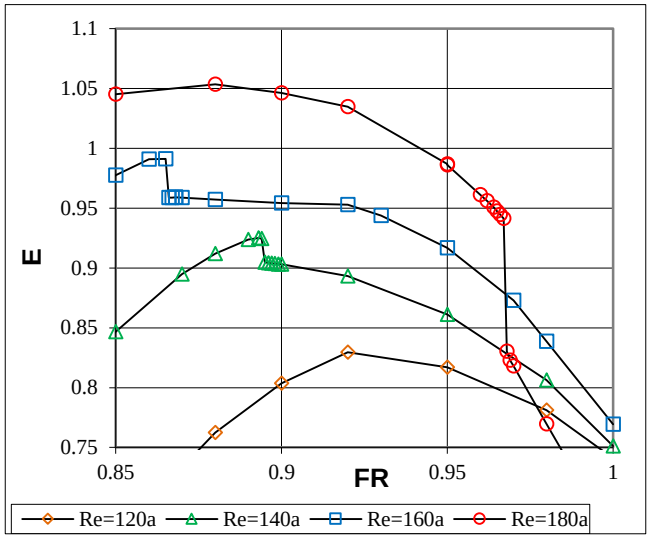

FIGURE 13: MECHANICAL ENERGY TRANSFER VS. FREQUENCY RATIO FOR ACW ORBIT AT DIFFERENT RE (ZOOM IN)

CONCLUSIONS

Forced two-degree of freedom cylinder motion in the shape of a figure-eight path (the cylinder placed across an otherwise uniform stream) was investigated for both clockwise (CW) and anticlockwise (ACW) directions of orbit in the upper loop of figure-eight in this two-dimensional numerical study. Mechanical energy transfer E between the cylinder and fluid, and time-mean (TM) and root-mean-square (rms) values of force coefficients were investigated against frequency ratio FR=f_y/St$_0$ in the lock-in domain up to FR=1 for Reynolds numbers Re=50 to 180. The computational procedure is based on the finite difference method and is thoroughly tested against experimental and numerical results available in the literature.

It was found that both Re and the direction of orbit have major effects on the force coefficients and the mechanical energy transfer. The major findings are as follows:

(1) The TM of lift was practically zero for ACW orbit for all values of Re. For CW orbit lift was also zero below around Re=100 irrespective of the FR value investigated. Above Re=100, however, the TM of lift is positive above a certain critical value of FR that decreases with Re. At Re=180 all TM values are positive in the investigated FR domain. Vortex contours for Re=180 at FR=0.85 showed vortex shedding mode P+S for the CW and 2S for the ACW orbit.

(2) The root-mean-square (rms) values of lift were much larger for the ACW case than for the CW case. The TM and rms of drag were not strikingly different for the two directions of orbit.
(3) As FR tends to unity no significant difference in the dynamics was detected for CW orbits or for ACW orbits below Re=140; above this jumps are seen in *E*, TM and rms of lift and drag for ACW orbits.
(4) *E* was negative for all Re values investigated for the CW orbit, meaning no potential danger of vortex-induced vibrations (VIV). For the ACW orbit however, *E* was positive over the large part of the parameter domain, increasing the potential risk of VIV for the equivalent free vibration case. Reducing Re reduces the value of *E* and with this, the risk of VIV.

Future research might include the investigation of phase angle between lift and transverse cylinder displacement which might shed some lights on these differences. The investigation of the effect of amplitude ratio (shape of the cylinder path) is continuing.

ACKNOWLEDGEMENTS

The work was carried out as part of the TÁMOP-4.2.1.B-10/2/ KONV-2010-0001 project in the framework of the New Hungarian Development Plan. The realization of this project is supported by the European Union, co-financed by the European Social Fund. Special thanks to L. Daróczy, designer of the flow visualization software (Fig. 5.).

REFERENCES

[1] Baranyi, L., 2008. "Numerical simulation of flow around an orbiting cylinder at different ellipticity values". *Journal of Fluids and Structures* **24**, pp. 883–906.
[2] Kheirkhah, S., Yarusevych, S., and Narasimhan, S., 2012. "Orbiting response in vortex-induced vibrations of a two-degree-of-freedom pivoted circular cylinder". *Journal of Fluids and Structures* **28**, pp. 343–358.
[3] Sanchis, A., Sælevik, G., and Grue, J., 2008. "Two-degree-of-freedom vortex-induced vibrations of a spring-mounted rigid cylinder with low mass ratio". *Journal of Fluids and Structures* **24**, pp. 907–919.
[4] Jeon, D., and Gharib, M., 2001. "On circular cylinders undergoing two-degree-of-freedom forced motions". *Journal of Fluids and Structures* **15**, pp. 533–541.
[5] Williamson, C.H.K., 2004. "Vortex-Induced Vibrations". *Annual Review of Fluid Mechanics* **36**, pp. 413–455.
[6] Leontini, J.S., Stewart, B.E., Thompson, M.C., and Hourigan, K., 2006. "Predicting vortex-induced vibration from driven oscillation results". *Applied Mathematical Modelling* **30**, pp. 1096–1102.
[7] Perdikaris, P.D., Kaiktsis, L., and Triantafyllou, G.S., 2009. "Computational study of flow structure and forces on a cylinder vibrating transversely and in-line to a steady stream: Effects of subharmonic forcing". In *Proc. ASME 2009 Pressure Vessels and Piping Conference, Symposium on Flow-Induced Vibration*. Paper No. PVP2009-78010, Prague
[8] Peppa, S., and Triantafyllou, G.S., 2016. "Sensitivity of two-dimensional flow past transversely oscillating cylinder to streamwise cylinder oscillations". *Physics of Fluids* **28**, pp. 037102-1 – 037102-16.
[9] Baranyi, L., 2012. "Simulation of a low-Reynolds number flow around a cylinder following a figure-8-path". *International Review of Applied Sciences and Engineering* **3**(2), pp. 133–146.
[10] Baranyi, L., 2015. "Effect of forced motion on the flow past circular cylinder following a figure-8 path". In Proceedings Conference on Modelling Fluid Flow (CMFF'15), J. Vad, ed., Budapest University of Technology and Economics, pp. 1-8. Paper Number CMFF15-057.
[11] Chakraborty, J., Verma, N., and Chhabra, R.P., 2004. "Wall effects in flow past a circular cylinder in a plane channel: a numerical study". *Chemical Engineering and Processing* **43**, pp. 1529–1537.
[12] Lu, X.Y., Dalton, C., 1996, "Calculation of the timing of vortex formation from an oscillating cylinder," *Journal of Fluids and Structures* **10**, pp. 527–541.
[13] Al-Mdallal, Q.M., Lawrence, K.P., and Kocabiyik, S., 2007. "Forced streamwise oscillations of a circular cylinder: Locked-on modes and resulting fluid forces". *Journal of Fluids and Structures* **23**, pp. 681–701.
[14] Didier, E., and Borges, A.R.J., 2007, "Numerical predictions of low Reynolds number flow over an oscillating circular cylinder," *Journal of Computational and Applied Mechanics* **8**, pp. 39–55.
[15] Posdziech, O., and Grundmann, R., 2007. "A systematic approach to the numerical calculation of fundamental quantities of the two-dimensional flow over a circular cylinder". *Journal of Fluids and Structures* **23**, pp. 479–499.
[16] Baranyi, L., 2005. "Lift and drag evaluation in translating and rotating non-inertial systems". *Journal of Fluids and Structures* **20**(1), pp. 25–34.
[17] Blackburn, H.M., and Henderson, R.D., 1999. "A study of two-dimensional flow past an oscillating cylinder". *Journal of Fluid Mechanics* **385**, pp. 255–286.
[18] Crawford, J.D., and Knobloch, E., 1991. "Symmetry and symmetry-breaking bifurcations in fluid dynamics". *Annual Review of Fluid Mechanics* **23**, pp. 341–387.
[19] Williamson, C.H.K., 1988. "Vortex formation in the wake of an oscillating cylinder". *Journal of Fluids and Structures* **2**, pp. 355–381.